Applied Catalysis B: Environmental 259 (2019) 118094

Contents lists available at ScienceDirect

Applied Catalysis B: Environmental

journal homepage: www.elsevier.com/locate/apcatb

Heterogeneous structural defects to prompt charge shuttle in g-C_3N_4 plane for boosting visible-light photocatalytic activity

Chengwu Yang[a,1], Zhe Xue[a,1], Jiaqian Qin[b,*], Montree Sawangphruk[c], Xinyu Zhang[a,*], Riping Liu[a]

[a] State Key Laboratory of Metastable Materials Science and Technology, Yanshan University, Qinhuangdao, 066004, PR China
[b] Research Unit of Advanced Materials for Energy Storage, Metallurgy and Materials Science Research Institute, Chulalongkorn University, Bangkok, 10330, Thailand
[c] Centre of Excellence for Energy Storage Technology (CEST), Department of Chemical and Biomolecular Engineering, School of Energy Science and Engineering, Vidyasirimedhi Institute of Science and Technology, Rayong, 21210, Thailand

ARTICLE INFO

Keywords:
Photocatalyst
g-C_3N_4
Heterogeneous structural defects
Charge shuttle
Hydrogen production

ABSTRACT

Structural defect engineering toward g-C_3N_4 plane usually has great benefit on modulating electron structure and photocatalytic performance. Here, we report a porous g-C_3N_4 material with heterogeneous structural defects, oxygen atom replacing edge nitrogen and cyano group, obtained via a facile treatment method. The reconstructed material shows narrowing band gap, high light absorption and fast charge separation. Theoretical calculation discloses that the doped oxygen atom and the nearby atoms accept electrons as reduction site to produce hydrogen, while the undoped fraction and cyano group take the duty to oxidize water. The delocalization of reactive sites drives charge shuttle on the plane, limiting recombination of charge carriers. Consequently, the modified g-C_3N_4 shows excellent photocatalytic activity with apparent quantum efficiency of 8.41% under 420 nm wavelength, surpassing pure g-C_3N_4 and other reported materials with defect compilation. We think that this work provides a new avenue to understand the function of structural defect on prompt charge separation.

1. Introduction

Photocatalytic technology is a promising means for energy conversion from solar to chemical energy. Polymeric graphitic carbon nitride (g-C_3N_4) as popular photocatalyst has attracted numerous attention in energy conversion due to the unique features, such as environmental benignity, good chemical stability, suitable bandgap to visible light absorption, proper band edge position to target reactants [1–3]. g-C_3N_4 has utilized in many kinds of photocatalytic domains, including hydrogen generation from water splitting, organic pollutant decomposition, and carbon dioxide reduction [4–6]. However, its limited light absorption ability and low separation efficiency of charge carriers result in low photocatalytic activity. Various strategies have been developed to amend drawbacks of g-C_3N_4, such as heteroatom doping [7,8], morphology optimization [9], heterojunction design [10,11] and dye sensitization [12]. Especially, introduction of structure defect into g-C_3N_4 plane was recently adopted as an efficient strategy to dramatically boost photocatalytic activity under visible light illumination. Structure defect in the g-C_3N_4 framework can not only adjust electronic distribution to narrow band gap for harvesting more visible light, but also work as new reactive sites participating into water splitting and prompt separation of photoexcited charge carriers. Atom vacancy and cyano group have been validated for enhancing photocatalytic activity up to date [13,14]. Approaches used to obtain cyano group include KOH-assisted polymerization of nitrogen-rich precursors, thermal treatment on pristine g-C_3N_4 nanosheets in high temperature or with reductant/oxidant [13,15–17]. These approaches inevitably bring intrinsic disadvantages, for example, high cost, low yield, difficult elimination of additives in the as-prepared material. Therefore, searching a new strategy to gift cyano group is very desirable. Besides, the doped heteroatom (e.g. boron, sulfur, oxygen, phosphorus, etc.) replacing carbon or nitrogen atom in the g-C_3N_4 lattice is a another kinds of structural defect, which often lead to lattice distortion and electron redistribution [18]. Heteroatom in lattice can spontaneously generate impurity energy level to tune band alignment of g-C_3N_4, and meanwhile establish charge trap center to suppress recombination of electron-hole pairs. Until now, many efforts only focus on single structural defect for enhancing photocatalytic activity of g-C_3N_4, rarely conceiving two or multiple structural defects in g-C_3N_4.

Hence, we design a novel organic acid-assisted method in this work

* Corresponding authors.
E-mail addresses: jiaqian.q@chula.ac.th (J. Qin), xyzhang@ysu.edu.cn (X. Zhang).
[1] These authors contributed equally to this work.

https://doi.org/10.1016/j.apcatb.2019.118094
Received 19 May 2019; Received in revised form 6 August 2019; Accepted 14 August 2019
Available online 14 August 2019
0926-3373/

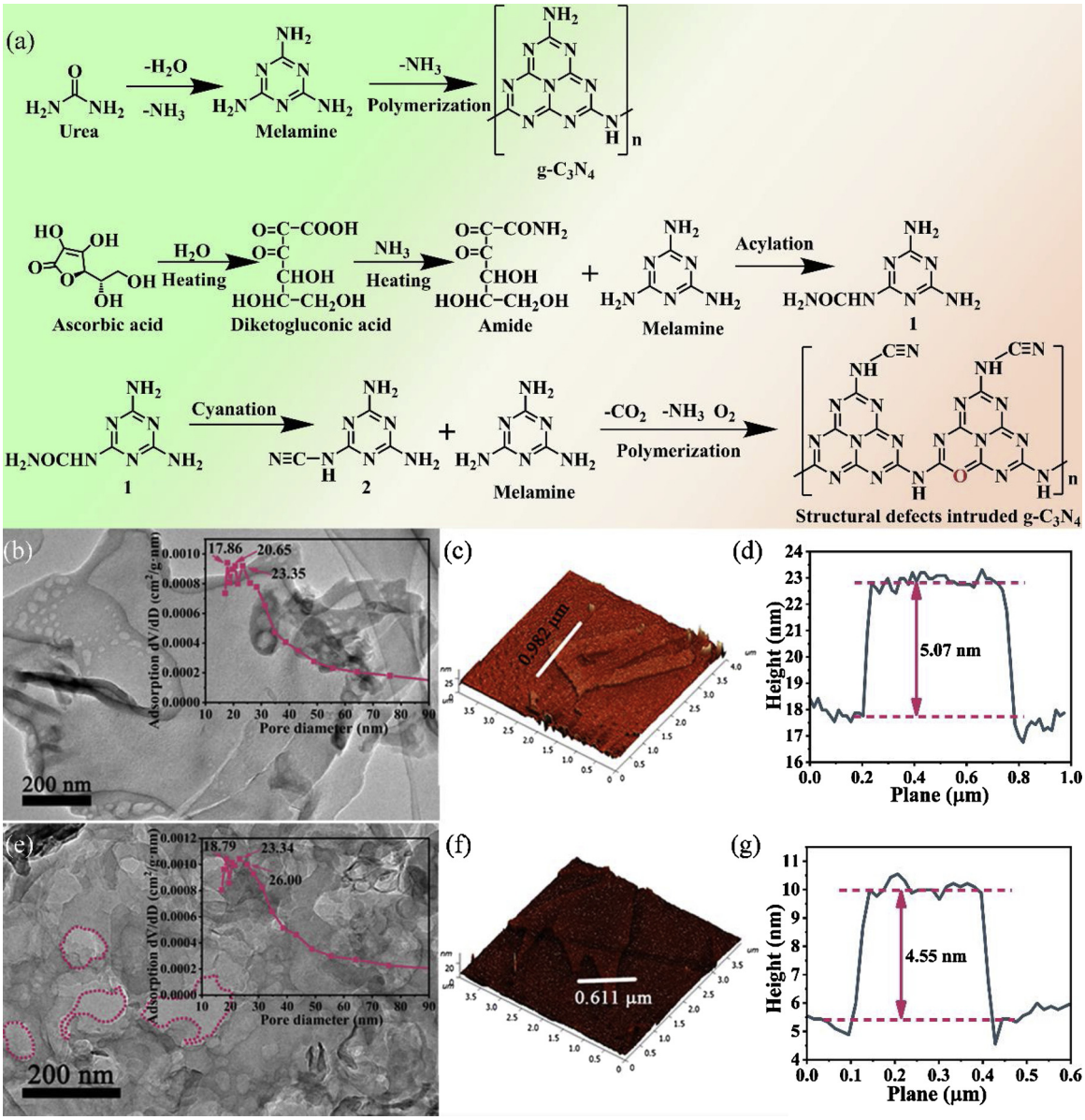

Fig. 1. (a) Reaction process of urea and ascorbic acid during heat treatment. (b) TEM image of GCN with pore diameter distribution calculated by BJH method. (c) AFM image of GCN and (d) the corresponding thickness analysis taken from the white line. (e) TEM image of COC30 with pore diameter distribution. (f) AFM image of COC30 and (g) the corresponding thickness analysis taken from the white line.

to synthesize a modified g-C_3N_4 by heterogeneous structural defects, which oxygen atom replacing edge nitrogen and cyano group are together incorporated into the plane. Heterogeneous defects in plane redshift light absorption onset and improve absorption capacity. Oxygen atom and cyano group delocalize reactive sites for splitting water and drive long-range migration of charge carrier, retarding charge recombination. Therefore, the modified g-C_3N_4 exhibits superior photocatalytic hydrogen activity under visible light. The measured apparent quantum efficiency on defective modified g-C_3N_4 reaches to 8.41%, exceeding that of g-C_3N_4 and other reported values. Thus, organic acid-assisted synthetic method presented here open a new avenue to produce heterogeneous structural defects on g-C_3N_4 plane and deeply understand the function of defect on prompt charge separation.

2. Results and discussion

The synthetic mechanism was described in Fig. 1a. At heating process, urea firstly releases ammonia gas and water molecule to form melamine and then polymerizes to pure g-C_3N_4 (GCN). The modified GCN can be synthesized by the calcination of the mixture of urea and ascorbic acid (ASA). In brief, urea (50 g) was first mixed with ASA and then treated with same heating process. The used amount of ASA was designed to be 10, 30, 50 and 70 mg, respectively. After cooling down, brown powders were obtained, which correspondingly signed as COC10, COC30, COC50 and COC70. However, for ASA can interact with water molecule released by urea to diketogluconic acid that can further react with ammonia gas via amidation [19–21]. Since oxygen and nitrogen atom possess stronger electronegative, the C—C bond between C = O and -$CONH_2$ in amide become active. The resultant amide reacts with melamine to form compound (1) via acylation [22]. Then, compound (1) lose a molecule of water and form compound (2) at high temperature via cyanation [23]. Cyano group is created at this reaction. Finally, compound (2) and melamine polymerize together at the presence of oxygen to synthesize the co-modified g-C_3N_4. The morphology of the as-prepared samples was first observed by scanning electron microscopy (SEM) and transmission electron microscopy (TEM). From

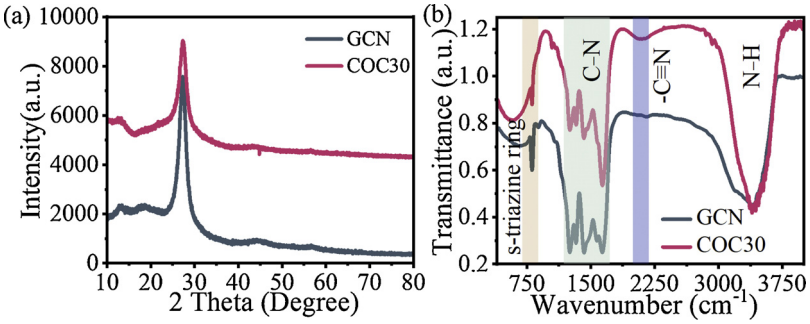

Fig. 2. (a) XRD patterns and (b) FTIR spectra of GCN and COC30.

SEM images (Fig. S1), GCN and COC30 possess an irregular and curved surface, which accords with the typical laminar morphology of carbon nitride. More clearly, observed from TEM, GCN nanosheets exhibit relatively intact morphology and distribute a small number of mesoporous with an average pore diameter of 13.1 nm (Fig. 1b), while the nanosheets are destroyed into fragment with an average pore distribution of 14.7 nm after undergoing ASA interference during urea polycondensation procedure (Fig. 1e). Simultaneously, the surface area significantly increases up to 55.8 m^2/g from 37.5 m^2/g for GCN. The optimized morphology trends to expose more active site to photocatalytic reaction. Nanosheet thickness was measured by atomic force microscopy (AFM). The thickness of GCN nanosheet is 5.07 nm (Fig. 1c and d), indicating that GCN nanosheet is consisted by ~16 C–N layers (the distance between two C–N atoms layers is about 0.33 nm). The corresponding value of COC30 decreases to 4.55 nm (Fig. 1f and g). This distinction elucidates that the number of atom layer in carbon nitride nanosheets is decreased after ASA interference, resulting in the enlarged distance of two nanosheets.

The crystallographic structure and phase composition were determined from X-ray diffraction (XRD) analysis, shown in Fig. 2a. Two distinct diffraction peaks can be found in the patterns for all the sample. The higher peak at 27.38° is indexed to (002) planes and ascribed to interplanar stacking of aromatic segments. The weak intensity peak at 13.32° is indexed to the (100) planes and represents the in-planar repeated tri-s-triazine units. The XRD pattern of modified g-C_3N_4 displays similar trends to that of unprocessed g-C_3N_4, proving that the fundamental crystal structure of g-C_3N_4 is preserved even after introducing defects. However, peak intensity of (002) planes decreases, probably because the distance between carbon nitride layers becomes large [24]. Fourier transform infrared (FTIR) spectra were employed to investigate the chemical structure of GCN and COC30 in Fig. 2b. The peaks between 800 and 1650 cm^{-1} are ascribed to the characteristic mode of s-triazine ring and C–N heterocycles [25]. The peak located at 3400 cm^{-1} is related to the N—H stretching deriving from the partial hydrogenation of nitrogen atoms in the nanosheets [26]. Noting that a new raised peak in FTIR spectrum of COC30 can be observed at 2140 cm^{-1} and identified as the stretching vibration of cyano group. The appearance of cyano group testifies the positive effect of ASA on defect formation.

The chemical environment and bonding state of GCN and COC30 were explored by X-ray photoelectron spectroscopy (XPS). GCN and COC30 consist of carbon, nitrogen and oxygen elements, judged from survey scan in Fig. S2. The high resolution XPS spectra of C1s, N1s and O1s were shown in Fig. 3a–c. Two major peaks at 284.6 and ~287.8 eV over C1s spectra of GCN and COC30 (Fig. 3a) can be attributed to the adventitious graphite carbon and sp^2-hybridized carbon in the C-$(N)_3$ atomic ring [11]. Interestingly, a minor peak is fitted at 286.13 eV for COC30, which is assigned to C–NH_x bonds on the edge of aromatic ring [13]. It can speculate that cyano group derived from the de-protonation of C–NH_x species via oxidation, because of the same binding energy of them. N1s spectra of GCN and COC30 can be divided into four deconvolution peaks at ~398.2, ~399.3, ~400.8 and ~403.9 eV, shown in Fig. 3b, which corresponds to sp^2 hybridized nitrogen C–N = C, tertiary nitrogen N-$(C)_3$, N—H bonds in the heptazine framework and π-excitations, respectively [27,28]. No new peak can be detected, but the bonding energies of all characteristic N1s peak exhibit an obvious red shift to higher values, reflecting the changed chemical environment and the reduced electron density of nitrogen atoms. The O1s spectra of GCN and COC30 have significant distinction as shown in Fig. 3c. Except a mutual fitted peak at ~531.9 eV for O—H bonds from water molecular, COC30 emits two emerging peak signal at 530.36 and 533.16 eV, which belong to N-C-O and C = O species in the lattice, respectively [7,27,29]. These results indicate that oxygen atoms can be incorporated into the g-C_3N_4 lattice to substitute the edge nitrogen sites. The stronger electronegativity of oxygen atoms than carbon and nitrogen endow the higher electron attracting capacity, which can decrease the electron density of carbon and nitrogen atoms and consequently result in right shift of binding energies on carbon and nitrogen. We calculated charge density difference of GCN and COC30 to explore such phenomenon (Fig. 3d). The doped oxygen atom distributes a tiny of charge, while the adjacent carbon and nitrogen atoms show the decreased density against before, which verifies the charge change visually and the right shift of binding energies. The C/N atom ratio is reduced from 0.738 for GCN to 0.727 for COC30. It matches well with structure change in CN heterocyclic ring. NMR measurement was adopted and provided further insight about chemical structure and bonding state (Fig. S3). Two intense peaks at 156.5 and 164.9 ppm are associated with the chemical structures of C_{3N} (1) and $C_{2N\text{-}NHx}$ (2) in the heptazine units, respectively [13]. It coincides to that of pure g-C_3N_4. Two other peaks at 124.8 and 177.9 ppm can be observed for COC30, which are ascribed to carbon atom in cyano group (3) and neighbor carbon atom (4) [30,31]. Notably, the peak intensities of C_{3N} and $C_{2N\text{-}NHx}$ on COC30 become lower than that of GCN, verifying that cyano group trend to appear at apex of melon structure following the de-protonation of C–NH_x species.

The actual photocatalytic activity for hydrogen production over different photocatalysts was evaluated under visible light illumination in TEOA aqueous solution. As shown in Fig. 4a, GCN exhibits a relatively low activity, yielding 106.9 μmol ·hydrogen production during 5 h. After loading structural defects, the photocatalytic activity gets obvious enhancement. COC30 photocatalyst meets the optimal performance, 334.2 μmol, which is about 3.1 times as high as that of GCN. This phenomenon demonstrates that defect modification is very effective to optimize the photocatalytic activity of pure g-C_3N_4. We measured the released hydrogen amount of GCN and COC30 under monochromatic light illumination with 420, 475 and 520 nm and calculated AQE values (Fig. 4b). The details of AQE calculation were given in Table S1. The hydrogen amount of COC30 is much greater than that of GCN as illuminated by 420 nm wavelength and the corresponding AQE value realize about five-fold increasing from 1.81% for GCN to 8.41% for COC30. The increased AQE under 420 nm light illumination also surpasses that of previous reported g-C_3N_4 based materials or other photocatalysts, summarized in Table S2. Moreover, COC30 produces 18.8 μmol hydrogen gas under 520 nm light illumination, while GCN is

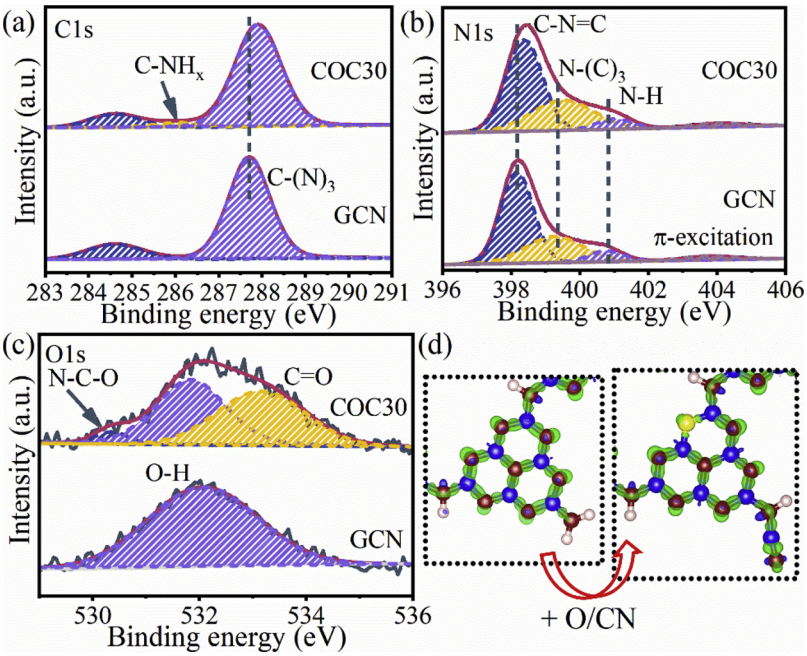

Fig. 3. The high resolution XPS spectra of (a) C1s, (b) N1s and (c) O1s for GCN and COC30. (d) Charge density difference comparison after loading oxygen atom and cyano group. The balls in blue, brown, yellow and pink denote carbon, nitrogen, oxygen and hydrogen atoms, respectively. (For interpretation of the references to colour in this figure legend, the reader is referred to the web version of this article).

inactive in this condition, indicating that g-C_3N_4 modified by structural defects possesses the optimized band gap and visible light response. The recycling hydrogen evolution experiment under visible light illumination was employed to characterize repeatability and stability of photocatalyst (Fig. 4c). Undergoing sequential photocatalytic reactions, COC30 remains same activity of splitting water, and oppositely, that of GCN decreased gradually. We further characterized structures and morphologies of GCN and COC30 after recycling via XRD and TEM to explain the reason. XRD patterns of GCN and COC30 are shown in Fig. S4a. The fundamental structure of GCN and COC30 has no big change after cyclic photocatalytic experiment. No characteristic peaks of Pt nanoparticles are observed on XRD patterns due to the low content in photocatalysts. The morphologies of GCN and COC30 are shown in Fig. S4b and c. The morphological features of GCN and COC30 are held

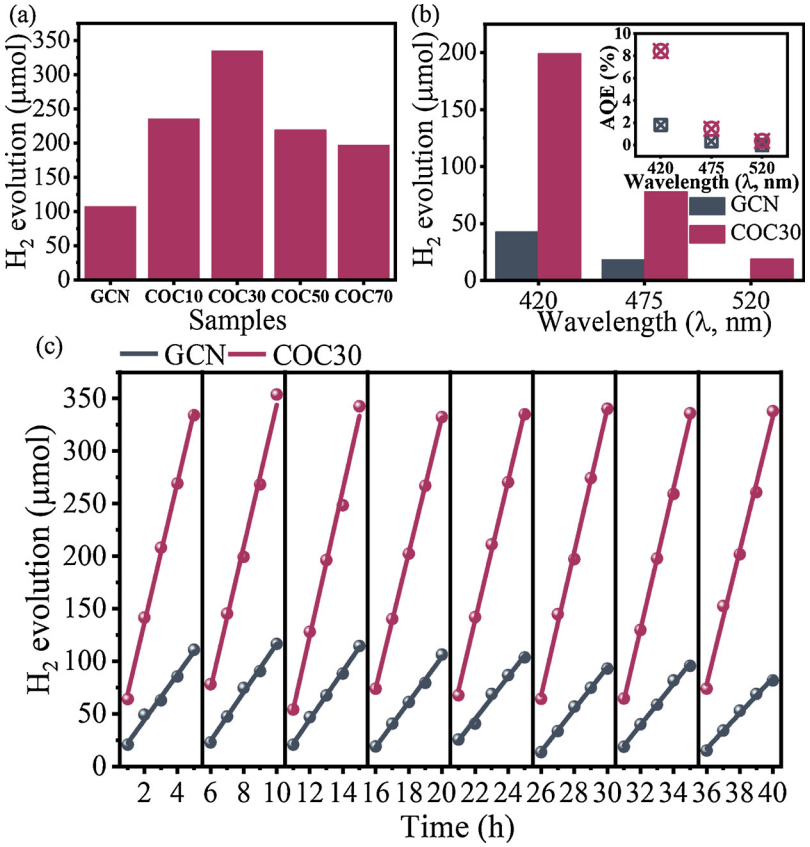

Fig. 4. (a) The photocatalytic generated hydrogen amount of GCN and COC30 under visible light illumination. (b) Hydrogen amount of GCN and COC30 under monochromatic light illumination with the corresponding AQEs in the inset figure. (c) The cycling photocatalytic hydrogen evolution of GCN and COC30 for 40 h.

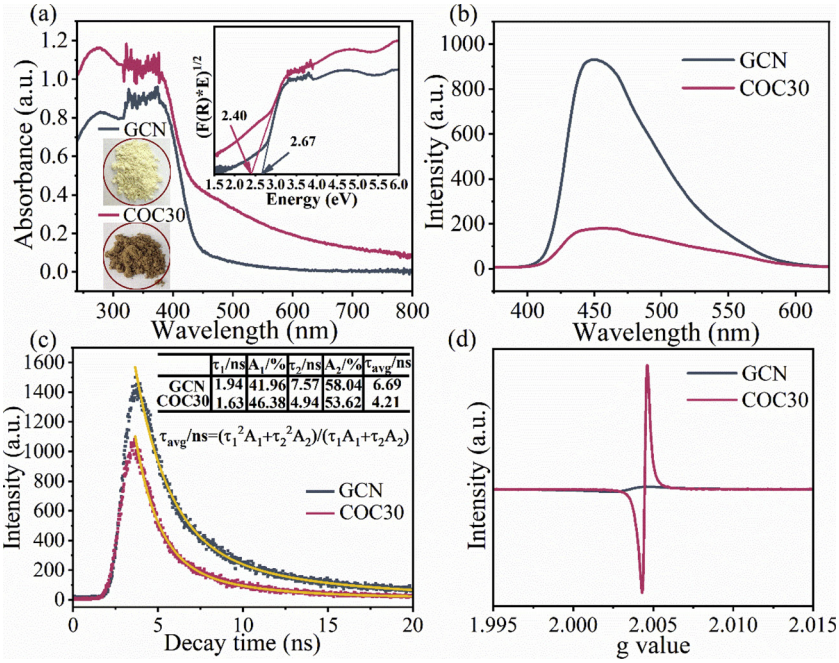

Fig. 5. (a) The diffusion reflectance spectra (DRS) of GCN and COC30 with band gap energy derived from Kubelka-Munk rule. The color of samples was shown in the images. (b) Photoluminescence (PL) spectra and (c) time-resolved photoluminescence (TRPL) decay spectra of GCN and COC30 for comparing charge separation efficiency. The calculated lifetime of charge carrier was implanted into the table. (d) Electron paramagnetic resonance (EPR) results measured under illumination.

consistent compared with before photocatalytic experiment. Pt nanoparticles via photodeposition are only loaded on the surface of nanosheets for GCN sample, implying the loose contact between Pt cocatalyst and g-C_3N_4 nanosheets. It easily results in the decreased photocatalytic activity during cyclic process, because Pt nanoparticles can gradually break away from g-C_3N_4 nanosheets. However, COC30 possesses the higher specific surface area and the larger pore diameter, which is convenient for Pt nanoparticles to load on the surface and insert into the interlayer, as shown in Fig. S4c. Such distribution can increase the contact level between Pt and photocatalyst. After recycling, the Pt content of COC30 is clearly higher than that of GCN. Thus, COC30 keeps more stable photocatalytic activity after continuous photocatalytic experiment.

Diffusion reflectance spectra (DRS) were used to determine the light absorption property of GCN and COC30 (Fig. 5a). Defects engineering alters the color to brown from pale yellow, which brings the higher light absorption ability in UV-VIS light band in a certain extent. Absorption peaks at 250–400 nm are caused by π–π* transitions in the conjugated heterocyclic systems [32]. An obvious absorption shoulder appearing at 420–600 nm reflects the su**b-g**ap feature due to excitation of mid-gap defect states originated from oxygen atom substitution [33]. The better light harvest of COC30 in this wave range accords with the variation tendency of photocatalytic activity between GCN and COC30 as monochromatic light illumination. A red shift toward absorption edge is found, indicating that the band gap of material is tuned. Based on Kubelka-Munk rule, the calculated band gap energies were shown in the inset figure. The band gap energies of GCN and COC30 are 2.67 and 2.40 eV, respectively, rendering the enhanced photon utilization efficiency. Photoluminescence (PL) emission spectra is a valid tool to analyze recombination behavior of charge carriers in photocatalyst (Fig. 5b). Differing from a strong fluorescence emission at 450 nm by GCN, COC30 presents a much quenched PL signals. This difference in principle indicates the fast separation of charge carriers in COC30 material. The introduced oxygen atoms create a mid-gap with the lower energy that can capture photoinduced electrons [34]. Besides, that nitrogen atom has a stronger electronegative than carbon atom makes cyano group with a typical electron-accepting character [35]. The advantage of capture effect to electrons by structural defects facilitates the migration and transfer of electrons across the plane and finally suppresses the recombination of electron-hole pairs [16]. The decreased lifetime of charge carriers measured by transient fluorescence spectra (Fig. 5c) implies that charge carriers can be more promptly captured by reactive substances, thus further evidencing the fast separation in COC30 [9]. Electron paramagnetic resonance (EPR) measurements were carried out to penetrate deep into recombination of charge carriers under light illumination (Fig. 5d). A symmetrical signal centers at g = 2.004 and corresponds to the unpaired electrons in π-conjugated carbon nitride heterocycles [36]. The sharper signal on COC30 contrasted to GCN indicates that COC30 can retard recombination of electron-hole pairs and produce more active electrons to participate in photocatalytic reaction process under light illumination. It benefits from structural defects of oxygen atoms and cyano group for redistributing the produce electrons in melon unit. These above results prove that oxygen atom and cyano group intruded synergistically into g-C_3N_4 is rational and efficient to optimize electron structure, enhance light response and reduce recombination of charge carriers.

Photoelectrochemical (PEC) performances of GCN and COC30 were assessed at 0.2 M Na_2SO_4 aqueous solution in the dark or irradiation. Photocurrent response via continuous on-off light cycles was shown in Fig. 6a. It can be seen that these two samples give a clear photocurrent with good increase as increasing potential. The photocurrent density growth of COC30 at every on-off light cycle is approximately 2 times that of GCN, indicating the better separation efficiency of photogenerated electrons and holes on COC30 and excellent reproducibility. Electrochemical impedance spectrosscopy (EIS) was also detected, shown in Fig. S5. COC30 exhibits a smaller arc radius compared with that of GCN in EIS plot, reflecting low internal electron resistance. It manifests that structural defects of oxygen atom and cyano group can reduce the resistance of g-C_3N_4 to accelerate migration of charge carriers across the plane. In order to determine band structure of GCN and COC30, we measured Mott-schottky (MS) plots from impedance potential test (Fig. 6b). These obtained MS plots show positive slope, representing the n-type semiconductor nature of GCN and COC30, meanwhile, the value of slope becomes small after introducing structural defects, suggesting the faster migration and separation of charges. Generally, flat band potential that is equivalent to the conduction band potential can be reckoned from the intersection between tangential line of MS plots and lateral axis. The flat band potentials of GCN and COC30 are -1.07 and -1.12 eV, respectively. The potential exhibits negative shift, which signifies that electrons in conduction band of COC30 are

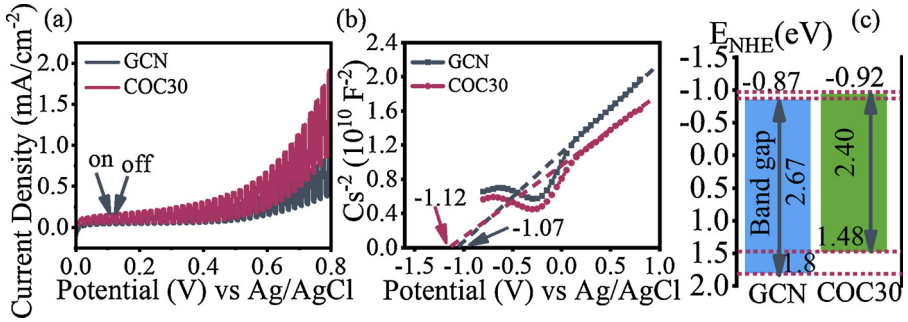

Fig. 6. Photoelectrochemical (PEC) results of GCN and COC30. (a) Transient photocurrent response measured under intermittent illumination. (b) Mottschottky (MS) plots with the flat band potential. (c) The obtained band alignment based on DRS and PEC results.

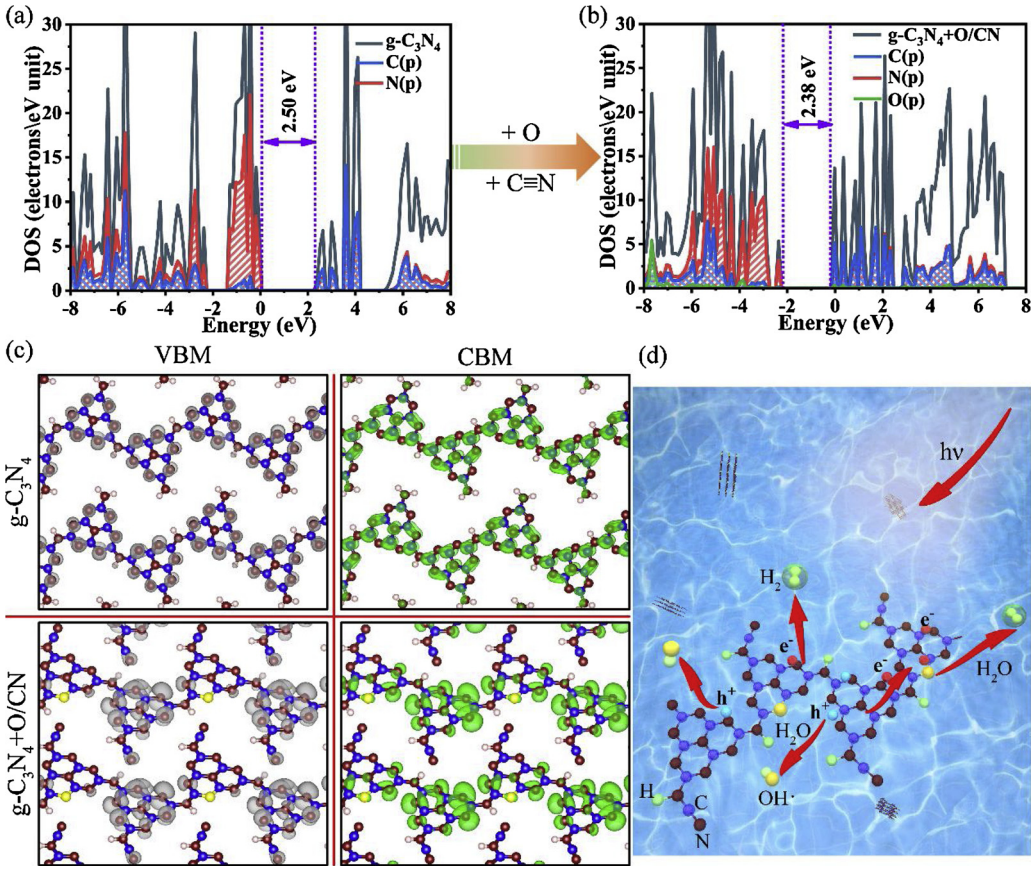

Fig. 7. The calculated projected density of states (PDOS) of (a) pure g-C_3N_4 and (b) the modified g-C_3N_4 via oxygen atom and cyano group. (c) The visual valence band maximum (VBM) and conduction band minimum (CBM) in the isosurface value of 0.002 eÅ^{-3}. (d) The proposed photocatalytic mechanism of the modified material about charge migration in different heptazine rings and the reactive site for splitting water. The balls in blue, brown, yellow, pink, red and cyan denote carbon, nitrogen, oxygen, hydrogen, electron and hole, respectively. (For interpretation of the references to colour in this figure legend, the reader is referred to the web version of this article).

more unstable and active, thus, easily split water. The calculated conduction band energies of GCN and COC30 are -0.87 and -0.92 eV, respectively, and the corresponding valance band energies are 1.8 and 1.48 eV according to band gap values. The band alignment was drawn in Fig. 6c. We supplemented ultraviolet photoelectron spectroscopy (UPS) to identify the correctness of band structure (Fig. S6). The valence band energies of GCN and COC30 in vacuum level are −6.1 and −5.7 eV, respectively. It is in line with the valence band energy versus normal hydrogen electrode from MS plots. So, the achieved band alignments are correct for GCN and COC30.

We obtained reasonable structure model about the structural defects modified g-C_3N_4 via DFT calculation, based on FTIR, XPS and NMR results. Six possible models (M1˜M6) were shown with system energy (Fig. S7). The lattice of all the models has no obvious distortion after oxygen substitution, because the similar atomic radius between oxygen and nitrogen atoms. It can be found that when oxygen atom closes to cyano group in same heptazine ring, system energy is increased and the corresponding model becomes unstable, which is determined by steric-hinerance effect from oxygen atom and cyano group. The energy of M6 structure is the lowest, suggesting that such model is reasonable for the synthetic materials. The calculated projected density of states (PDOS) of pure g-C_3N_4 and the modified g-C_3N_4 were shown in Fig. 7a and b. The simulated band gaps of g-C_3N_4 and the modified material are 2.50 and 2.38 eV, respectively, coinciding with the experimental values. It evidences that structural defects, oxygen atom and cyano group, can effectively optimize band gap of g-C_3N_4. The valence band (VB) of g-C_3N_4 is constituted by the atomic orbital of N2p, and the conduction band (CB) is occupied by the atomic orbitals of C2p and N2p. Differently, for defects modified g-C_3N_4, the CB contain minor component of O2p orbital, implying that the doped oxygen atom also takes the roles for reduction reaction site. Hence, we further analyze valence band maximum (VBM) and conduction band minimum (CBM) in the isosurface value of 0.002 eÅ^{-3} (Fig. 7c). Observed from VBM of g-C_3N_4, the charges disperse in the edge nitrogen of heptazine ring. These atoms can excite electrons to CB and produce holes under illumination, acting as oxidation sites for water to hydroxyl radical [37,38]. In CBM of g-

C_3N_4, carbon atoms and the center nitrogen accept charges as reduction sites [32]. The redox reaction sites locate in one heptazine ring, limiting the long-range migration of charge and quickening recombination of electron-hole pairs. This configuration is adverse for photocatalytic performance. However, VBM and CBM of defects modified g-C_3N_4 are obviously differ from these of pure g-C_3N_4. From VBM, nitrogen atoms and cyano group in the undoped heptazine ring dominate the major charges and can donate photoexcited electrons to CB, acting as oxidation sites. From CBM, oxygen atom and the nearby nitrogen atoms in doped fraction receive electron to reduce water. It is worth noting that the bridge nitrogen atoms linking heptazine rings possess charge in the both VBM and CBM images, disclosing that a shuttling channel is formed to facilitate charge migration in different heptazine rings via bridge nitrogen [39]. The delocalized redox reaction sites prompt spatial separation of electrons and holes and drive charge migration in different heptazine rings, finally hampering recombination of charge. The water decomposition process was drawn in Fig. 7d, where water oxidation to hydroxyl radical occurs in the undoped heptazine (nitrogen atoms and cyano group) and hydrogen gas is generated from the doped fraction (oxygen atom and the nearby nitrogen). Therefore, it can conclude that the change of electronic structure between pure and modified g-C_3N_4, originating from oxygen atom and cyano group, play a vital role in controlling photocatalytic activity.

3. Conclusions

In summary, we designed a facile method to synthesize novel g-C_3N_4 based material modified by heterogeneous structural defects. Oxygen atom substituting edge nitrogen in heptazine ring and cyano group were together introduced into g-C_3N_4 plane. The structural defects modified g-C_3N_4 possesses narrowing band gap, excellent light absorption capacity and charge separation efficiency. The introduction of oxygen atom and cyano group leads to delocalization of reactive sites for splitting water and drives charge shuttle between different heptazine rings, revealing by theoretical calculation. As a result, the photocatalytic activity for hydrogen production after modification achieves prominent enhancement, where AQE under 420 nm wavelength is up to 8.41%, exceeding that of g-C_3N_4 and other reported values.

Declaration of Competing Interest

The authors declare that they have no known competing financial interests or personal relationships that could have appeared to influence the work reported in this paper.

Acknowledgements

This work is supported by Thailand Research Fund (RSA6080017), and the Energy Conservation Promotion Fund from and the Energy Policy and Planning Office, Ministry of Energy. We also gratefully acknowledge the NSFC (grant 51421091), and National Science Foundation for Distinguished Young Scholars for Hebei Province of China (grant E2016203376), and Asahi Glass Foundation.

Appendix A. Supplementary data

Supplementary material related to this article can be found, in the online version, at doi:https://doi.org/10.1016/j.apcatb.2019.118094.

References

[1] W.-J. Ong, L.-L. Tan, Y.H. Ng, S.-T. Yong, S.-P. Chai, Graphitic carbon nitride (g-C3N4)-based photocatalysts for artificial photosynthesis and environmental remediation: are we a step closer to achieving sustainability? Chem. Rev. 116 (2016) 7159–7329.
[2] X. Wang, K. Maeda, A. Thomas, K. Takanabe, G. Xin, J.M. Carlsson, K. Domen, M. Antonietti, A metal-free polymeric photocatalyst for hydrogen production from water under visible light, Nat. Mater. 8 (2008) 76.
[3] V.W. Lau, V.W. Yu, F. Ehrat, T. Botari, I. Moudrakovski, T. Simon, V. Duppel, E. Medina, J.K. Stolarczyk, J. Feldmann, V. Blum, B.V. Lotsch, Urea-modified carbon nitrides: enhancing photocatalytic hydrogen evolution by rational defect engineering, Adv. Eng. Mater. 7 (2017) 1602251.
[4] H. Zhang, L. Zhao, F. Geng, L.-H. Guo, B. Wan, Y. Yang, Carbon dots decorated graphitic carbon nitride as an efficient metal-free photocatalyst for phenol degradation, Appl. Catal. B: Environ 180 (2016) 656–662.
[5] J. Liu, Y. Liu, N. Liu, Y. Han, X. Zhang, H. Huang, Y. Lifshitz, S.-T. Lee, J. Zhong, Z. Kang, Metal-free efficient photocatalyst for stable visible water splitting via a two-electron pathway, Science 347 (2015) 970.
[6] P. Xia, B. Zhu, J. Yu, S. Cao, M. Jaroniec, Ultra-thin nanosheet assemblies of graphitic carbon nitride for enhanced photocatalytic CO2 reduction, J. Mater. Chem. A 5 (2017) 3230–3238.
[7] Z.-F. Huang, J. Song, L. Pan, Z. Wang, X. Zhang, J.-J. Zou, W. Mi, X. Zhang, L. Wang, Carbon nitride with simultaneous porous network and O-doping for efficient solar-energy-driven hydrogen evolution, Nano Energy 12 (2015) 646–656.
[8] S. Guo, Z. Deng, M. Li, B. Jiang, C. Tian, Q. Pan, H. Fu, Phosphorus-doped carbon nitride tubes with a layered micro-nanostructure for enhanced visible-light photocatalytic hydrogen evolution, Angew. Chem. Int. Ed. 55 (2016) 1830–1834.
[9] N. Tian, Y. Zhang, X. Li, K. Xiao, X. Du, F. Dong, G.I.N. Waterhouse, T. Zhang, H. Huang, Precursor-reforming protocol to 3D mesoporous g-C3N4 established by ultrathin self-doped nanosheets for superior hydrogen evolution, Nano Energy 38 (2017) 72–81.
[10] L. Kong, X. Zhang, C. Wang, J. Xu, X. Du, L. Li, Ti3+ defect mediated g-C3N4/TiO2 Z-scheme system for enhanced photocatalytic redox performance, Appl. Surf. Sci. 448 (2018) 288–296.
[11] C. Yang, Z. Xue, J. Qin, M. Sawangphruk, S. Rajendran, X. Zhang, R. Liu, Visible Light-Driven Photocatalytic H2 Generation and Mechanism Insights into Bi2O2CO3/G-C3N4 Z-Scheme Photocatalyst, J. Phys. Chem. C 123 (2019) 4795–4804.
[12] J. Qin, J. Huo, P. Zhang, J. Zeng, T. Wang, H. Zeng, Improving the photocatalytic hydrogen production of Ag/g-C3N4 nanocomposites by dye-sensitization under visible light irradiation, Nanoscale 8 (2016) 2249–2259.
[13] H. Yu, R. Shi, Y. Zhao, T. Bian, Y. Zhao, C. Zhou, G.I.N. Waterhouse, L.-Z. Wu, C.-H. Tung, T. Zhang, Alkali-assisted synthesis of nitrogen deficient graphitic carbon nitride with tunable band structures for efficient visible-light-Driven hydrogen evolution, Adv. Mater. 29 (2017) 1605148.
[14] P. Niu, G. Liu, H.-M. Cheng, Nitrogen vacancy-promoted photocatalytic activity of graphitic carbon nitride, J. Phys. Chem. C 116 (2012) 11013–11018.
[15] Y. Wen, D. Qu, L. An, X. Gao, W. Jiang, D. Wu, D. Yang, Z. Sun, Defective g-C3N4 prepared by the NaBH4 reduction for high-performance H2 production, ACS Sustain. Chem. Eng. 7 (2019) 2343–2349.
[16] P. Niu, M. Qiao, Y. Li, L. Huang, T. Zhai, Distinctive defects engineering in graphitic carbon nitride for greatly extended visible light photocatalytic hydrogen evolution, Nano Energy 44 (2018) 73–81.
[17] D. Zhang, Y. Guo, Z. Zhao, Porous defect-modified graphitic carbon nitride via a facile one-step approach with significantly enhanced photocatalytic hydrogen evolution under visible light irradiation, Appl. Catal. B: Environ 226 (2018) 1–9.
[18] X. Liu, L. Dai, Carbon-based metal-free catalysts, Nat. Rev. Mater. 1 (2016) 16064.
[19] T. Narendar Reddy, A. Beatriz, V. Jayathirtha Rao, D.P. de Lima, Carbonyl compounds′ journey to amide bond formation, Chem. Â€ “Asian J. 14 (2019) 344–388.
[20] I. Kreituss, J.W. Bode, Catalytic kinetic resolution of saturated N-heterocycles by enantioselective amidation with chiral hydroxamic acids, Acc. Chem. Res. 49 (2016) 2807–2821.
[21] B.M. Dorr, D.E. Fuerst, Enzymatic amidation for industrial applications, Curr. Opin. Chem. Biol. 43 (2018) 127–133.
[22] A.I. Fernández-Llamazares, J. Spengler, F. Albericio, Review backbone N-modified peptides: how to meet the challenge of secondary amine acylation, Pept. Sci. 104 (2015) 435–452.
[23] N.-u.H. Khan, R.I. Kureshy, S.H.R. Abdi, S. Agrawal, R.V. Jasra, Metal catalyzed asymmetric cyanation reactions, Coord. Chem. Rev. 252 (2008) 593–623.
[24] H. Ou, L. Lin, Y. Zheng, P. Yang, Y. Fang, X. Wang, Tri-s-triazine-based crystalline carbon nitride nanosheets for an improved hydrogen evolution, Adv. Mater. 29 (2017) 1700008.
[25] L. Zhang, N. Ding, L. Lou, K. Iwasaki, H. Wu, Y. Luo, D. Li, K. Nakata, A. Fujishima, Q. Meng, Localized surface plasmon resonance enhanced photocatalytic hydrogen evolution via Pt@Au NRs/C3N4 nanotubes under visible-light irradiation, Adv. Funct. Mater. 29 (2019) 1806774.
[26] X. Chen, R. Shi, Q. Chen, Z. Zhang, W. Jiang, Y. Zhu, T. Zhang, Three-dimensional porous g-C3N4 for highly efficient photocatalytic overall water splitting, Nano Energy 59 (2019) 644–650.
[27] J. Li, B. Shen, Z. Hong, B. Lin, B. Gao, Y. Chen, A facile approach to synthesize novel oxygen-doped g-C3N4 with superior visible-light photoreactivity, Chem. Commun. (Camb.) 48 (2012) 12017–12019.
[28] S. Yang, Y. Gong, J. Zhang, L. Zhan, L. Ma, Z. Fang, R. Vajtai, X. Wang, P.M. Ajayan, Exfoliated graphitic carbon nitride nanosheets as efficient catalysts for hydrogen evolution under visible light, Adv. Mater. 25 (2013) 2452–2456.
[29] L. Ming, H. Yue, L. Xu, F. Chen, Hydrothermal synthesis of oxidized g-C3N4 and its regulation of photocatalytic activity, J. Mater. Chem. A 2 (2014) 19145–19149.
[30] J. Yuan, X. Liu, Y. Tang, Y. Zeng, L. Wang, S. Zhang, T. Cai, Y. Liu, S. Luo, Y. Pei, C. Liu, Positioning cyanamide defects in g-C3N4: Engineering energy levels and active sites for superior photocatalytic hydrogen evolution, Appl. Catal. B: Environ 237 (2018) 24–31.
[31] V.W.-h. Lau, I. Moudrakovski, T. Botari, S. Weinberger, M.B. Mesch, V. Duppel, J. Senker, V. Blum, B.V. Lotsch, Rational design of carbon nitride photocatalysts by

identification of cyanamide defects as catalytically relevant sites, Nat. Commun. 7 (2016) 12165.
[32] R. You, H. Dou, L. Chen, S. Zheng, Y. Zhang, Graphitic carbon nitride with S and O codoping for enhanced visible light photocatalytic performance, RSC Adv. 7 (2017) 15842–15850.
[33] L.K. Putri, B.-J. Ng, W.-J. Ong, H.W. Lee, W.S. Chang, S.-P. Chai, Engineering nanoscale p–n junction via the synergetic dual-doping of p-type boron-doped graphene hybridized with n-type oxygen-doped carbon nitride for enhanced photocatalytic hydrogen evolution, J. Mater. Chem. A 6 (2018) 3181–3194.
[34] X. Chen, L. Liu, P.Y. Yu, S.S. Mao, Increasing solar absorption for photocatalysis with black hydrogenated titanium dioxide nanocrystals, Science 331 (2011) 746.
[35] G. Liu, G. Zhao, W. Zhou, Y. Liu, H. Pang, H. Zhang, D. Hao, X. Meng, P. Li, T. Kako, J. Ye, In situ bond modulation of graphitic carbon nitride to construct p–n homojunctions for enhanced photocatalytic hydrogen production, Adv. Funct. Mater. 26 (2016) 6822–6829.
[36] S. Zhang, C. Hu, H. Ji, L. Zhang, F. Li, Facile synthesis of nitrogen-deficient mesoporous graphitic carbon nitride for highly efficient photocatalytic performance, Appl. Surf. Sci. 478 (2019) 304–312.
[37] H. Yang, R. Cao, P. Sun, X. Deng, S. Zhang, X. Xu, Highly dispersed and noble metal-free MPX (M = Ni, Co, Fe) coupled with g-C3N4 nanosheets as 0D/2D photocatalysts for hydrogen evolution, Appl. Surf. Sci. 458 (2018) 893–902.
[38] R. Cao, H. Yang, X. Deng, P. Sun, S. Zhang, X. Xu, Construction of 3DOM carbon nitrides with quasi-honeycomb structures for efficient photocatalytic H2 production, ChemCatChem 10 (2018) 5656–5664.
[39] H. Yang, R. Cao, P. Sun, J. Yin, S. Zhang, X. Xu, Constructing electrostatic self-assembled 2D/2D ultra-thin ZnIn2S4/protonated g-C3N4 heterojunctions for excellent photocatalytic performance under visible light, Appl. Catal. B: Environ 256 (2019) 117862.